eLIFE
elifesciences.org

Figures and figure supplements

Resting state functional connectivity in the human spinal cord

Robert L Barry, et al.

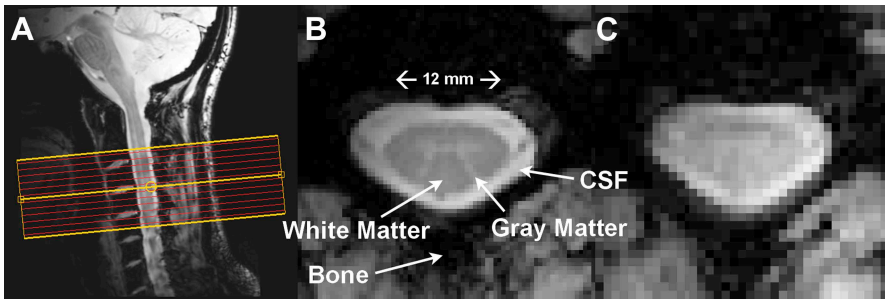

Figure 1. Resting state spinal cord fMRI at 7 Tesla. (**A**) Mid-sagittal slice from a healthy volunteer showing the complete cervical cord and typical axial slice placement for this resting state study. In all subjects the imaging stack was centered on the C3/C4 junction, providing full coverage of C3 and C4 and partial coverage of C2 and C5. (**B**) T_2^*-weighted anatomical image at C4 acquired with 0.6 × 0.6 × 4 mm^3 voxels and interpolated to 0.31 × 0.31 × 4 mm^3. Excellent contrast permits visualization of the characteristic butterfly-shaped gray matter column. (**C**) A single T_2^*-weighted functional image of this axial slice (acquired with 0.91 × 0.91 × 4 mm^3 voxels). Functional images are high quality with minimal geometric distortions and T_2^* blurring and permit adequate spatial delineation between white matter and cerebrospinal fluid.

DOI: 10.7554/eLife.02812.003

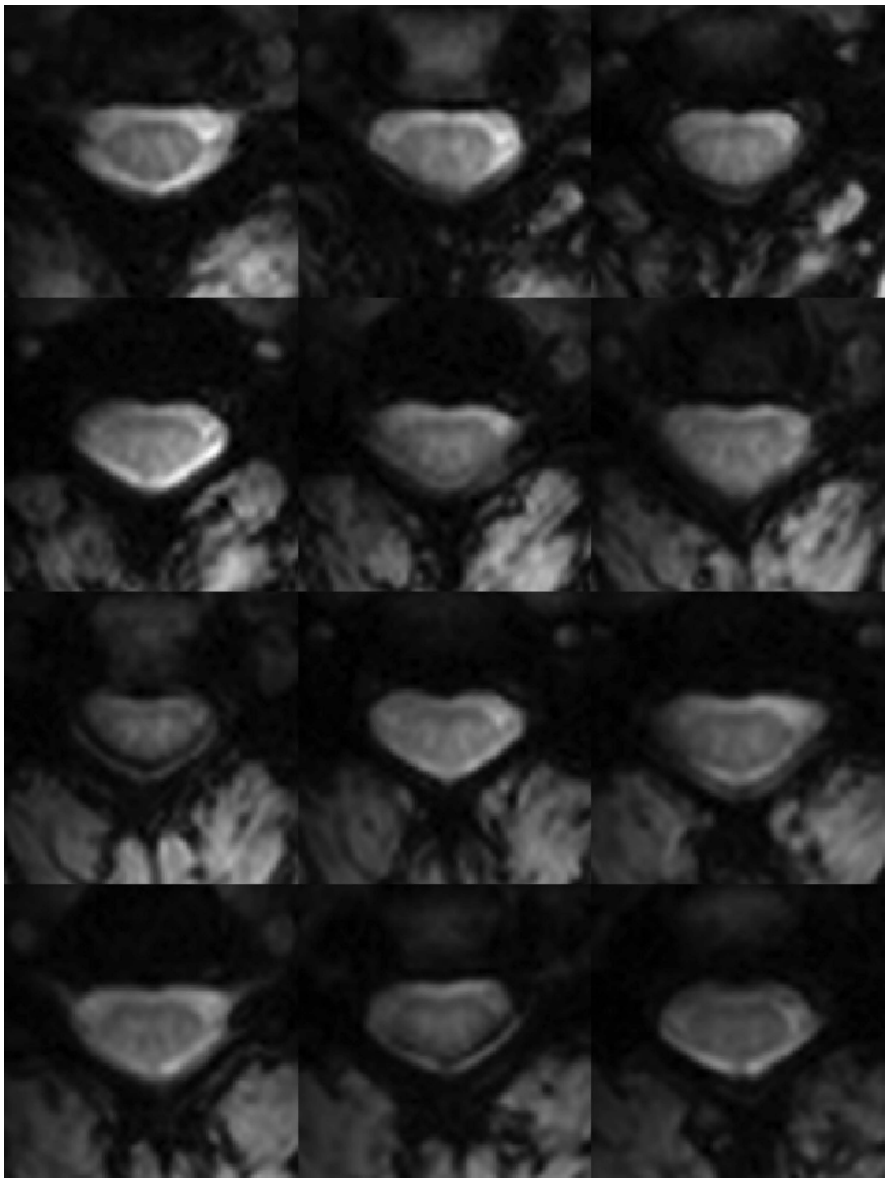

Figure 2. Functional weighted spinal cord images at 7 Tesla. A single volume of twelve contiguous T_2*-weighted slices centered on the C3/C4 junction (as illustrated in ***Figure 1A***) in one subject. Each volume was acquired with 0.91 × 0.91 × 4 mm^3 voxels and resampled to 0.31 × 0.31 × 4 mm^3 voxels during the affine functional-to-anatomical registration. Excellent contrast between white matter and cerebrospinal fluid facilitates accurate registration between such functional volumes and high-resolution anatomical images (***Figure 1B***). The use of a 3D acquisition sequence with relatively short echo time and relatively few k-space lines per radiofrequency pulse provides high-quality images with minimal signal drop-out and geometric distortions, although artifacts caused by fat shift of the nerve root sleeve in the phase-encode direction still affect the dorsal edge in a few slices.

DOI: 10.7554/eLife.02812.004

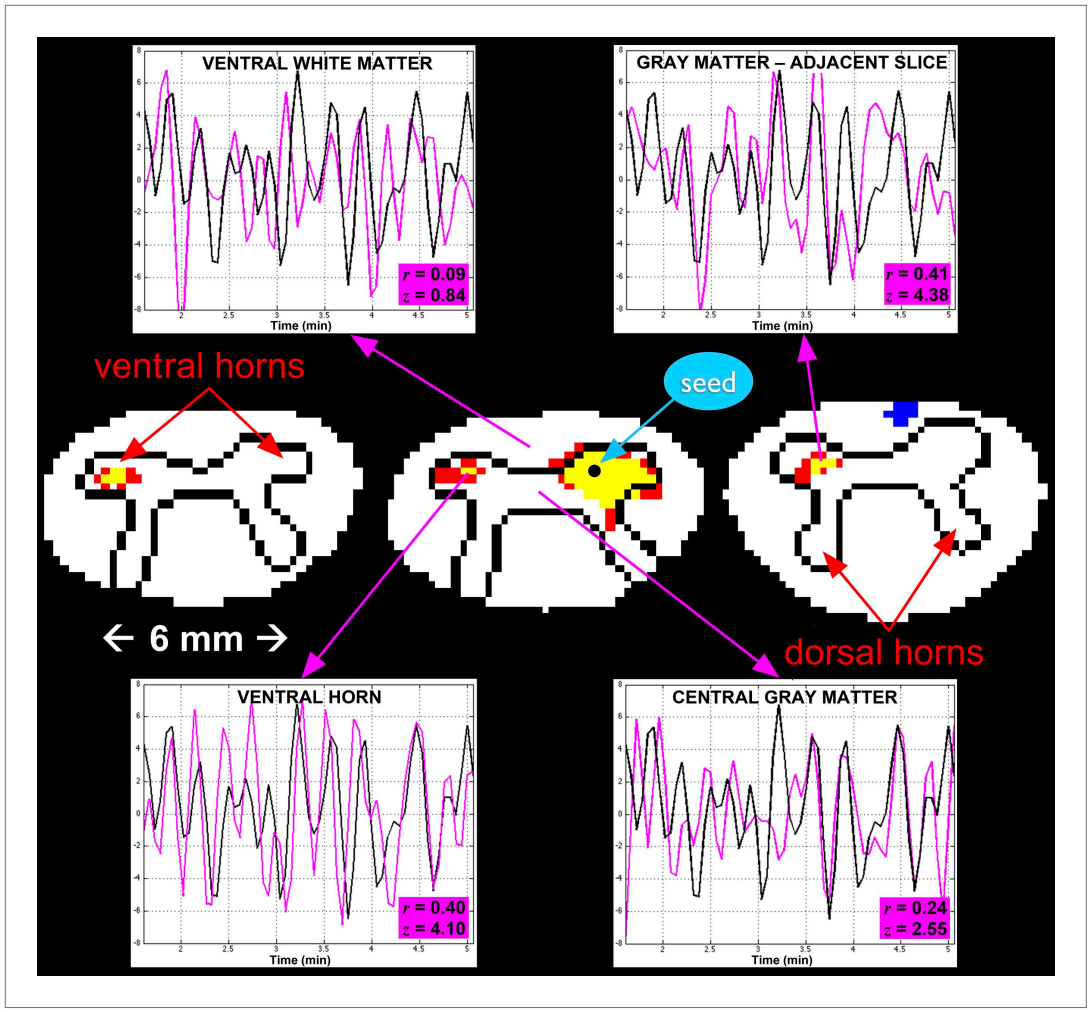

Figure 3. A single-subject analysis of resting state functional connectivity with corresponding time series. For clarity, only outlines of the gray matter butterfly and surrounding white matter are shown (rostro-caudal from left to right). Red and yellow represent statistically significant positive correlation with the seed time series (using a two-sided 99.9% confidence interval where red is $3.29 < z \leq 3.89$ and yellow is $z > 3.89$), and blue represents negative correlation ($z < -3.29$). The seed voxel is selected in the right ventral horn in C5, and exhibits functional connectivity with the contralateral ventral horn in the same slice as well as adjacent slices. Such connectivity between ventral horns is observed across all subjects. In each of the four plots, a 3.5-min segment of the seed time course is shown in black and the time course of the corresponding region of interest is shown in magenta. The highest correlations are observed in the contralateral ventral horn on the same slice ($z = 4.10$) and on the adjacent slices ($z = 4.38$). Correlations with central gray matter ($z = 2.55$) and adjacent white matter ($z = 0.84$) are relatively low, which, given the small size of the spinal cord, suggest that such correlations are genuine and not dominated by widespread physiological noise.

DOI: 10.7554/eLife.02812.005

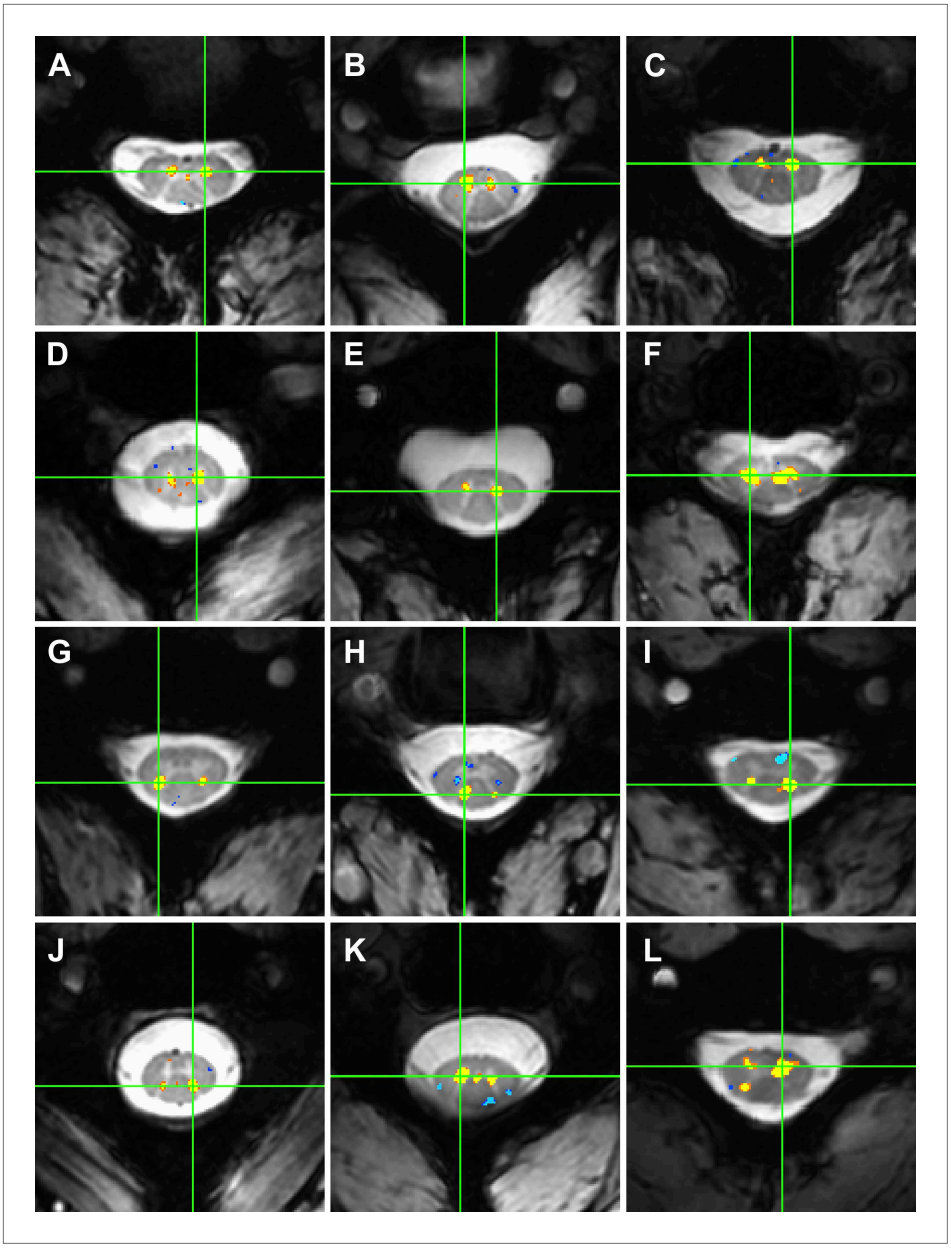

Figure 4. Examples of within-slice resting state functional connectivity across subjects. These analyses were performed using AFNI's 'InstaCorr' with $p < 0.001$ and no minimum cluster size. In each panel, a seed voxel is marked with a green crosshair and resultant correlations are overlaid on the anatomical image. (**A**)–(**F**) Connectivity between ventral horns for subjects 1, 3, 8, 10, 11, and 13, respectively. (**G**)–(**J**) Connectivity between dorsal horns for subjects 5, 16, 18, and 22, respectively. (**K** and **L**) Less common correlations within gray matter. In (**K**) (subject 20), focal connectivity between ventral horns and with central gray matter. In (**L**) (subject 7), connectivity between ventral horns but also with the contralateral dorsal horn. At the single-subject level, there is some evidence for functional connectivity between ventral and dorsal horns, but such correlations are less common across slices and not statistically significant at the group level.

DOI: 10.7554/eLife.02812.006

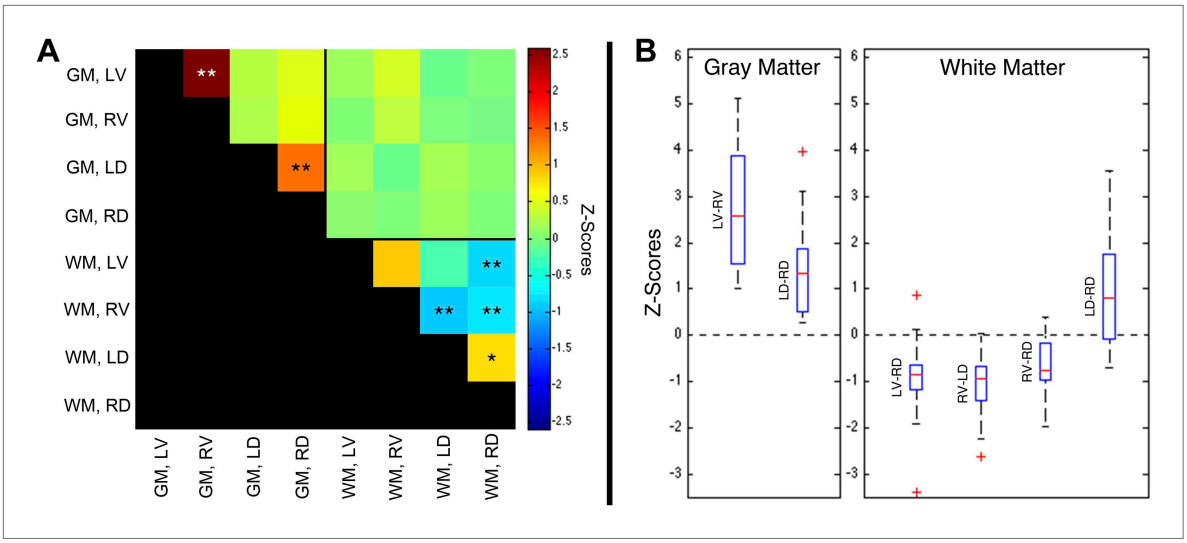

Figure 5. Group-level functional connectivity between sub-regions of spinal gray matter (GM) and surrounding white matter (WM) within slices. (**A**) In GM, strong positive correlations are observed between left (LV) and right (RV) ventral horns, as well as left (LD) and right (RD) dorsal horns (*p<0.05; **p<0.01; Bonferroni corrected). Weaker positive and negative correlations are observed within WM. No statistically significant correlations are observed between spinal GM and WM (upper right quadrant). (**B**) Box-and-whisker plots showing the median and upper and lower quartiles of the six statistically significant results identified in (**A**). Whiskers extend out to 1.5 times the distance between the upper and lower quartiles, and an outlier (beyond the whiskers) is denoted by a plus. Wilcoxon signed rank tests identify the distributions of *z*-scores (across all slices and subjects) that are significantly different from zero ($p < 0.05$). Functional connectivity between WM sub-regions is more variable and exhibits both positive and negative median correlations. In comparison, median GM correlations between LV-RV and LD-RD are positive across all 22 subjects. Additional analysis permutations (described in ***Figure 5—figure supplements 1, 3, and 5*** with example GM power spectra shown in ***Figure 5—figure supplements 2, 4, and 6***) reveal that the three negative WM correlations are influenced by WM regression (step #12) and thus are open to more than one interpretation. However, supplementary analyses reveal that the positive GM correlations between ventral horns and between dorsal horns persist across all preprocessing permutations. These additional analyses further support the conclusion that positive correlations between GM horns are not artifactual—possibly created by preprocessing choices or frequency bandwidth selection—and most likely represent genuine functional connectivity.

DOI: 10.7554/eLife.02812.007

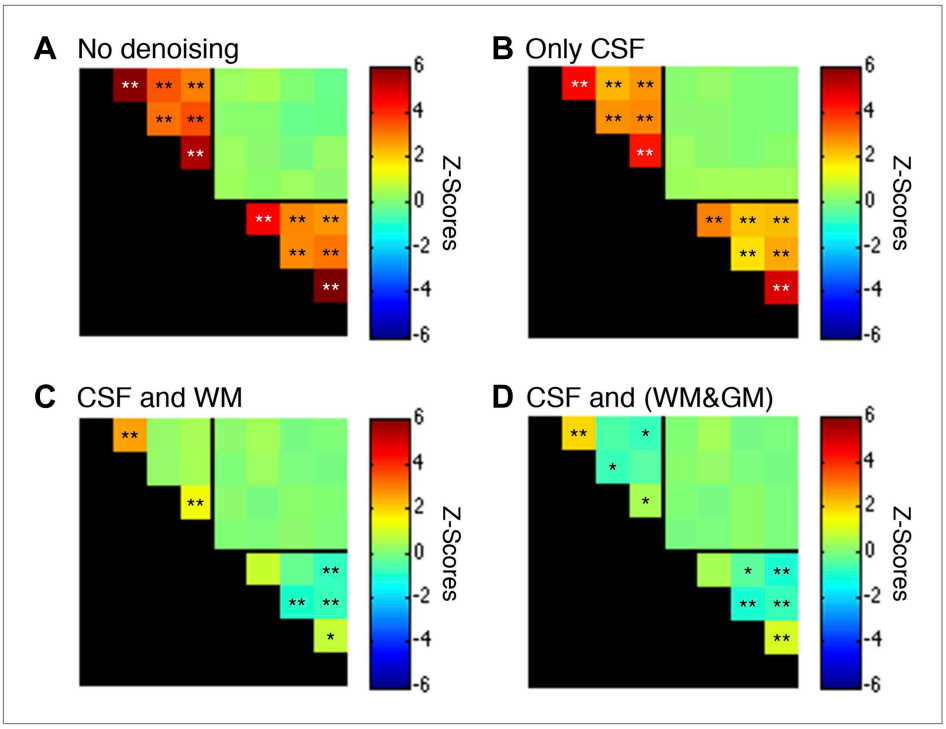

Figure 5—figure supplement 1. Functional connectivity matrices resulting from preprocessing pipeline permutations.

DOI: 10.7554/eLife.02812.009

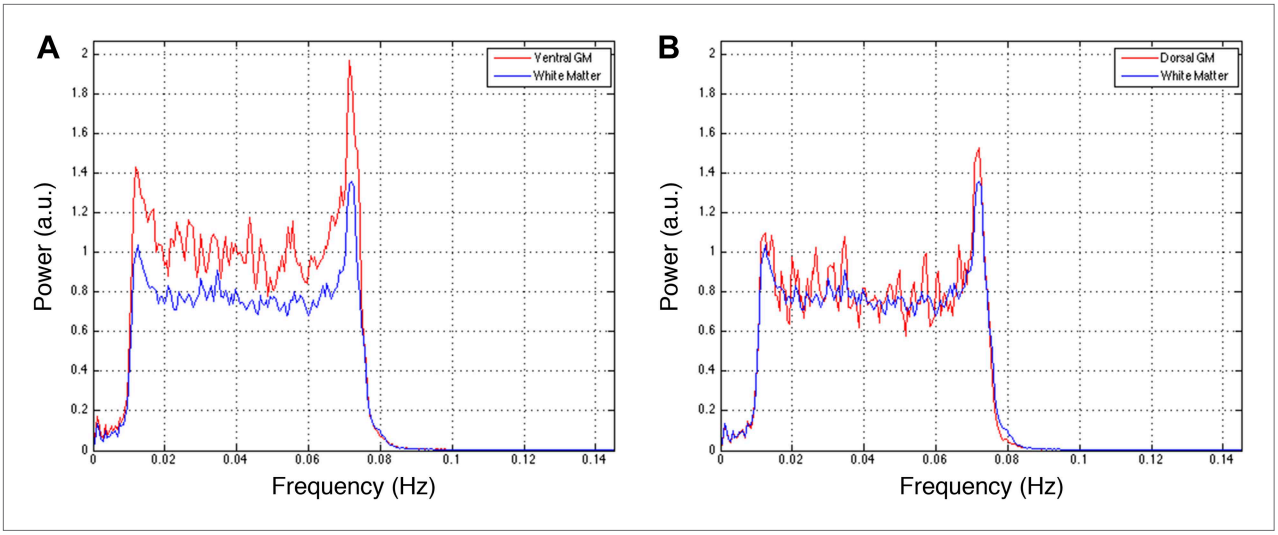

Figure 5—figure supplement 2. Power spectra across gray and white matter sub-regions for data filtered between 0.01 and 0.08 Hz.

DOI: 10.7554/eLife.02812.010

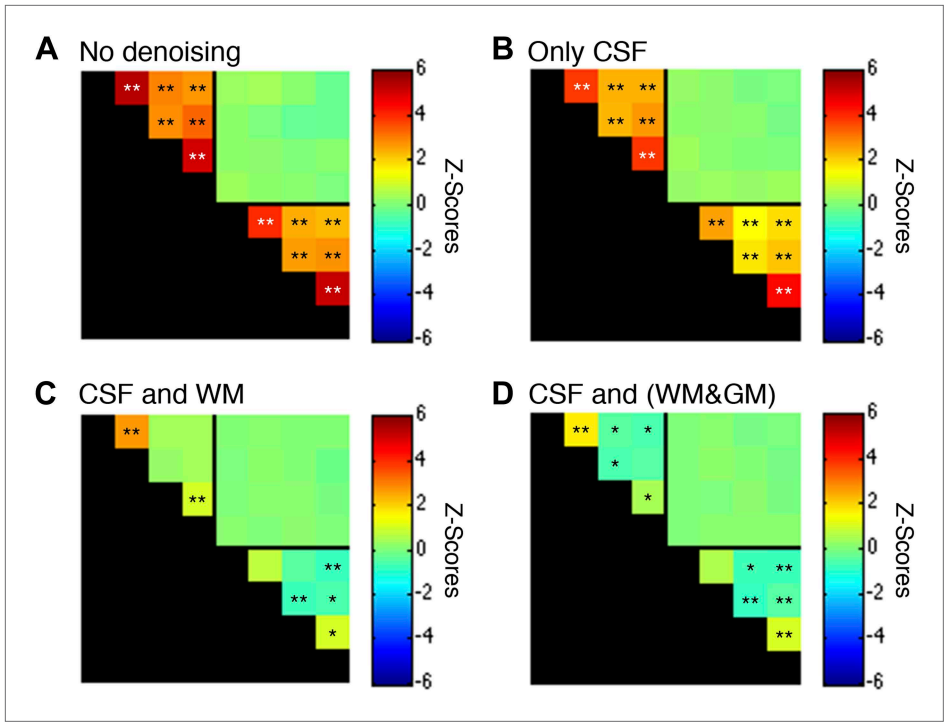

Figure 5—figure supplement 3. Functional connectivity matrices resulting from preprocessing pipeline permutations after band-pass filtering between 0.01 and 0.07 Hz.
DOI: 10.7554/eLife.02812.011

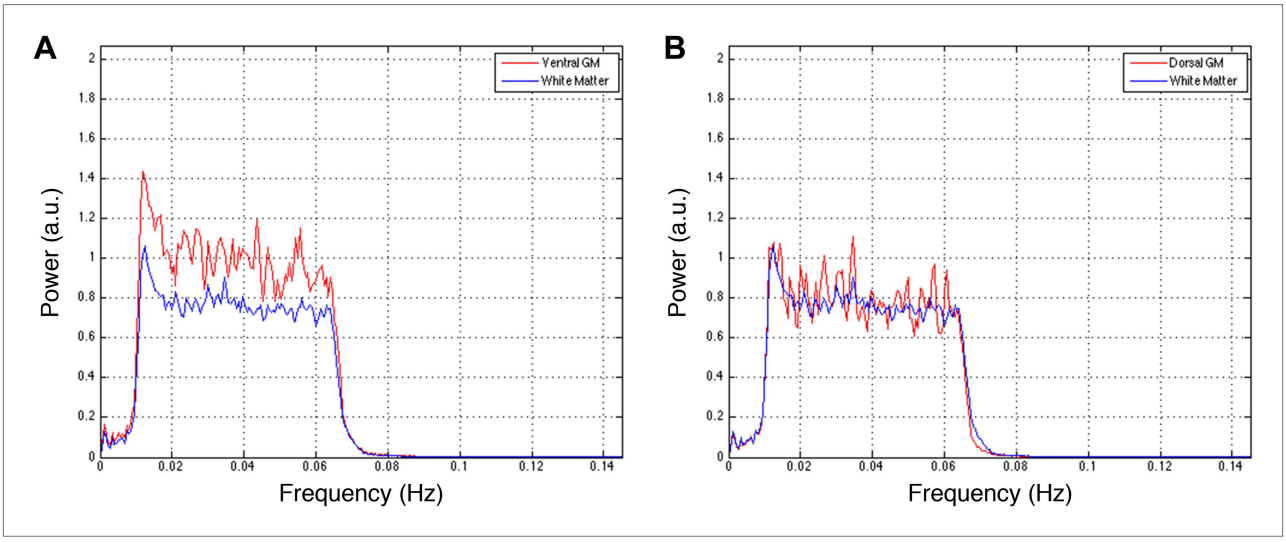

Figure 5—figure supplement 4. Power spectra across gray and white matter sub-regions for data filtered between 0.01 and 0.07 Hz.
DOI: 10.7554/eLife.02812.012

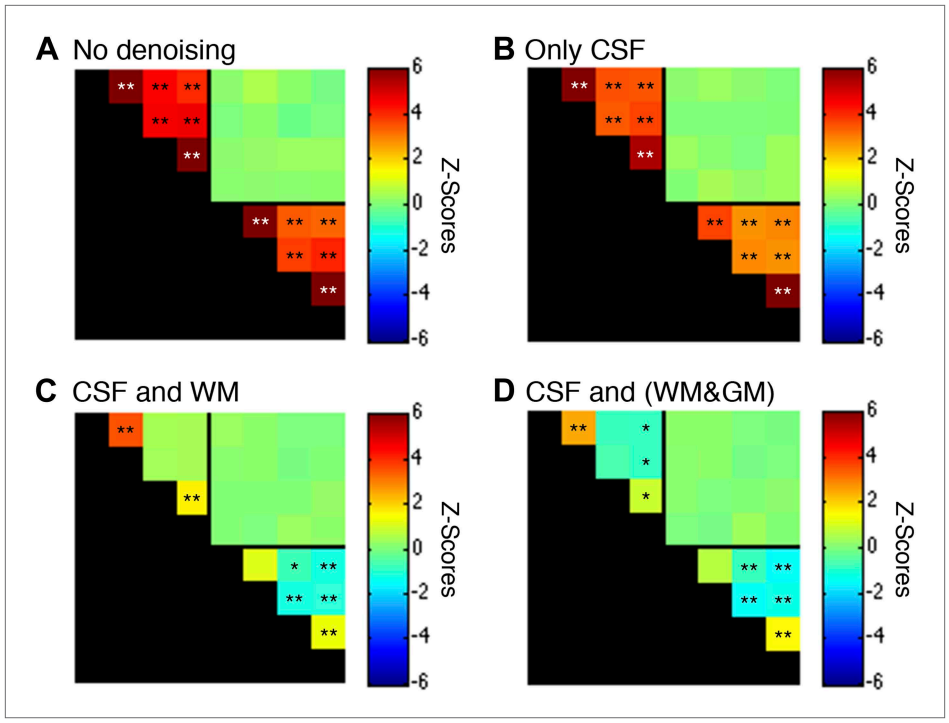

Figure 5—figure supplement 5. Functional connectivity matrices resulting from preprocessing pipeline permutations after band-pass filtering between 0.01 and 0.13 Hz.
DOI: 10.7554/eLife.02812.013

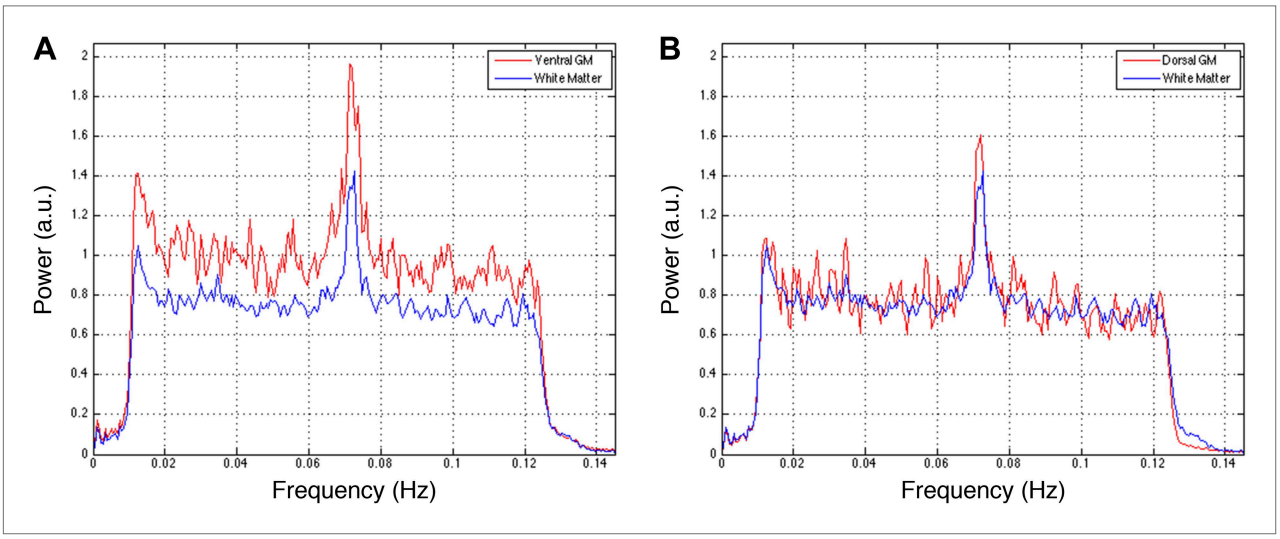

Figure 5—figure supplement 6. Power spectra across gray and white matter sub-regions for data filtered between 0.01 and 0.13 Hz.
DOI: 10.7554/eLife.02812.014